The Cryosphere Discuss., 6, 4205–4231, 2012
www.the-cryosphere-discuss.net/6/4205/2012/
doi:10.5194/tcd-6-4205-2012

The Cryosphere Discussions

Theoretical study of solar light reflectance from vertical snow surfaces

O. V. Nikolaeva[1] **and A. A. Kokhanovsky**[2]

[1]Institute of Applied Mathematics, Moscow, Russia
[2]Institute of Environmental Physics, Bremen University, O. Hahn Allee 1, 28334 Bremen, Germany

Received: 27 July 2012 – Accepted: 9 August 2012 – Published: 1 October 2012

Correspondence to: A. A. Kokhanovsky (alexk@iup.physik.uni-bremen.de)

Published by Copernicus Publications on behalf of the European Geosciences Union.

Abstract

The influence of horizontal and vertical inhomegeneity of snow surfaces on solar light reflectance is studied using the radiative transfer theory (RTT). We found that large errors are produced if the 1-D RTT is used for the calculation of snow reflection function (and, therefore, also in the retrievals of the snow grain radii) in 3-D measurement geometries. Such 3-D geometries are common in the procedures for the determination of the effective snow grain radii using near infrared photography and spectroscopy of vertical snow walls.

1 Introduction

Optical measurements are commonly used to derive snow microphysical parameters from plane-parallel snow layers (Kokhanovsky et al., 2011). In particular, snow grain size is obtained from the near infrared (NIR) measurements (in the spectral range 865–1240 nm) of intensity of solar light reflected from flat snow layers. The physical background of the retrieval is the enhancement of light absorption by larger ice grains (and as a consequence, a smaller light reflectance for snow layers with larger grains). The main problem with such a method that only upper snow layers (say, up to 5 cm or so in depth) can be observed. The information on the snow microphysical parameters and snow pollution in deeper layers can not be retrieved because of high absorption of NIR radiation by snow grains. As a matter of fact, NIR radiation does not penetrate deep into snowpack and, therefore, does not bring information on the properties of snow from the depths above 5 cm or so. To avoid this problem recently measurements along the vertical snow walls become popular (see, e.g. Fig. 1 in Matzl and Schneebeli, 2006, and Fig. 2 in Painter et al., 2007). Also measurements along the length of cylindrical holes in snow are used (Barker and Korolev, 2010; Arnaud et al., 2011). In all these papers the 1-D transfer theory is used for the interpretation of results and determination of snow grain sizes. Although there could be some influences of 3-D effects on corresponding

TCD
6, 4205–4231, 2012

measurements. The aim of this work is twofold. Firstly, we develop a software, which can be used for studies of 3-D effects in snow and, secondly, we study corresponding 3-D effects (shadowing, enhancement of brightness, etc.).

The paper is structured as follows. In the next section we introduce the radiative transfer equation and boundary conditions relevant to the studies of light propagation in snow. The numerical algorithm developed for the solution of corresponding integro – differential equation is described in Sect. 3. The results of numerical experiments are reported in Sect. 4.

2 Theory

It is assumed that surface of snow is flat (no sastrugi, no microstructures on the snow surface), snowpack is a layered turbid medium (layers have different sizes of grains and levels of pollution). We simulate the case of a wide pit (1–3 m wide and 0.5–0.7 m in depth) in a snowpack. Clearly, the radiative transfer in such a region is influenced by such wide openings in snow. In particular, the shadowing and brightening effects can play an important role. Therefore, we assume in our numerical experiment that the pit is covered by a tent to reduce direct light effects. Although even in this case 3-D effects of light transport near the snow wall can not be neglected.

The scheme of the corresponding experiment for the case of a pit, covered by a sheer film, that forms the diffuse light source, is shown in Fig. 1. Such a source corresponds to real conditions of measurements. Reflected radiation is registered on the vertical side of the pit and the top boundary of the snowpack. The opposite side and the bottom of the pit can be covered by black film, see Figs. 2–4, to reduce influence of these surfaces on registered intensity of these surfaces.

Because a region under consideration has the symmetry plane, all problems can be considered in the 2-D framework. The following transport equation for the radiance I

TCD
6, 4205–4231, 2012

should be solved

$$\frac{\partial I}{\partial \mathbf{\Omega}} + \sigma(x,z) I(x,z,\theta,\phi)$$
$$= \sigma(x,z)\, \omega_0(x,z) \int_0^{\pi} d\theta'\, \sin\theta' \int_0^{2\pi} d\phi'\, I(x,z,\theta',\phi')\, \rho(x,z,\theta,\phi,\theta',\phi') \quad (1)$$

in the region $[0, X] \times [0, H]$, see Fig. 5. The pit $[0, R] \times [0, H]$ is filled by air, whereas the medium out of the pit is snow. Then one has for extinction coefficient

$$\sigma(x,z) = \begin{cases} \sigma^{\text{air}} & \text{as } x \le R \\ \sigma^{\text{snow}} & \text{as } x > R \end{cases}, \quad (2)$$

for single scattering albedo

$$\omega_0(x,z) = \begin{cases} \omega_0^{\text{air}} & \text{as } x \le R \\ \omega_0^{\text{snow}}(z) & \text{as } x > R \end{cases}, \quad (3)$$

for scattering phase function

$$\rho(x,z,\theta,\phi,\theta',\phi') = \begin{cases} \rho^{\text{air}} & \text{as } x \le R \\ \rho^{\text{snow}}(z) & \text{as } x > R \end{cases} \quad (4)$$

Note, the single scattering albedo $\omega_0^{\text{snow}}(z)$ is considered as piece-wise function of depth, that describes a layered snowpack, the special case $\omega_0^{\text{snow}}(z) = \text{const}$ corresponds to a homogeneous snow layer. Horizontal width X of the region is taken so that 1-D slab regime, when radiation intensity depends only on height coordinate z, is valid far from the pit.

TCD
6, 4205–4231, 2012

The bottom boundary $z = 0$ is a Lambertian surface with albedo $A(x)$:

$$I(x,0,\theta,\phi)|_{\cos\theta>0} = \hat{R}[I] = A(x)\frac{1}{\pi}\int_{\pi/2}^{\pi} d\theta' \sin\theta' |\cos\theta'| \int_{0}^{2\pi} d\phi' I(x,0,\theta',\phi'). \quad (5)$$

Black condition is defined on the right boundaries $x = X$

$$I(X,z,\theta,\phi)|_{\cos\phi<0} = 0. \quad (6)$$

Reflecting condition with albedo A_s is defined on the left boundary $x = 0$

$$I(0,z,\theta,\phi)|_{\cos\phi>0} = A_s I(0,z,\theta,\pi-\phi). \quad (7)$$

The diffuse source on the top boundary is imposed in a way

$$I(x,H,\theta,\phi)|_{\cos\theta<0} = S_0\frac{1}{4\pi}, \quad (8)$$

where S_0 is the incident light irradiance.

Depending on albedo A_s and $A(x)$ the Eqs. (5) and (7) model different physical regions. Under $A_s = 1$, $A(x) \equiv A^{\text{snow}} = 0.8$ one has 3-D snowpack with the pit of the diameter D, see Fig. 1. In such a case radiation is reflected by the two sides and bottom of the pit.

Under $A_s = 1$, $A(x) = \begin{cases} 0 & \text{as } x \le R, \\ A^{\text{snow}} & \text{else,} \end{cases}$ the bottom of this pit is covered by black film and radiation is reflected only by the pit's sides, see Fig. 2.

Under $A_s = 0$, $A(x) = \begin{cases} 0 & \text{as } x \le R, \\ A^{\text{snow}} & \text{else,} \end{cases}$ the bottom and one side of this pit are covered by black film, see Fig. 3, radiation is reflected only by one side of the pit.

TCD
6, 4205–4231, 2012

3 Numerical algorithm

The problem in Eqs. (1–8) under the diffuse source should be solved via a numerical method to find the reflected radiation intensity. Let outline the numerical method developed by us for the solution of the corresponding 2-D problem. First introduce a quadrature with nodes $\mathbf{\Omega}_m\{\theta_m,\phi_m\}$, see Fig. 5, and weights $\Delta\Omega_m$, $m = 1,\ldots M$. Then approximate the continuous function $I(x,z,\theta,\phi)$ by functions $I_m(x,z) = I(x,z,\theta_m,\phi_m)$ and replace the scattering integral in the Eq. (1) by the quadrature sum

$$\int_0^{\pi} d\theta' \, \sin\theta' \int_0^{2\pi} d\phi' \, I(x,z,\theta',\phi') \, \rho(x,z,\theta_m,\phi_m,\theta',\phi') \cong \sum_{n=1}^{M} I_n(x,z) \, \rho_{nm},$$

$$\rho_{nm} = \int_{\Delta\Omega_n} d\phi' \, d\theta' \, \sin\theta' \, \rho(x,z,\theta_m,\phi_m,\theta',\phi'). \tag{9}$$

Therefore, the problem is reduced to a system of differential equations. The coefficients ρ_{nm} correspond to the scattering event from direction $\mathbf{\Omega}_n\{\theta_n,\phi_n\}$ to direction $\mathbf{\Omega}_m\{\theta_m,\phi_m\}$ and are integrals containing a complicated forward-peaked phase function. They can be found by a quadrature sum

$$\rho_{nm} = \sum_{j=1}^{L_n} \Delta\Omega_{j,n} \, \rho(x,z,\theta_m,\phi_m,\theta_{j,n},\phi_{j,n}), \tag{10}$$

where the nodes $\Omega_{j,n}(\theta_{j,n},\phi_{j,n})$ and the weights $\Delta\Omega_{j,n}$ define an additional quadrature over the node $\Delta\Omega_n$. The following equality is kept

$$\sum_{j=1}^{L_n} \Delta\Omega_{j,n} = \Delta\Omega_n. \tag{11}$$

TCD
6, 4205–4231, 2012

This quadrature is adapted into the integrand function reducing in the region $\Delta\Omega_n$ according to variation of the function being integrated, see Fig. 6.

To solve the differential equations system for the functions $I_m(x,z)$, introduce a regular mesh over spatial variables x, z

$$0 = x_{1/2} < \ldots < x_{k+1/2} < \ldots < x_{K+1/2} = X, \quad (12)$$

$$0 = z_{1/2} < \ldots < z_{j+1/2} < \ldots < z_{J+1/2} = H. \quad (13)$$

Each cell $[x_{k-1/2}, x_{k+1/2}] \times [z_{j-1/2}, z_{j+1/2}]$ with steps $\Delta x_k = x_{k+1/2} - x_{k-1/2}$, $\Delta z_j = z_{j+1/2} - z_{j-1/2}$ is considered as a homogeneous one. Integrating the Eq. (1) over this cell, one obtains the exact algebraic relation

$$\xi_m (I_{m,k+1/2,j} - I_{m,k-1/2,j})/\Delta x_k + \gamma_m (I_{m,k,j+1/2} - I_{m,k,j-1/2})/\Delta z_j + \sigma_{k,j} I_{m,k,j} = 0, \quad (14)$$

where values

$$\xi_m = \sin\theta_m \cos\phi_m, \quad \gamma_m = \cos\theta_m \quad (15)$$

are projections of the unit vector $\mathbf{\Omega}_m$ onto coordinates axes x and z, see Fig. 5.

Values $I_{m,k,j}$, $I_{m,k\pm1/2,j}$, $I_{m,k,j\pm1/2}$ are averaged intensity over a cell and over its edges

$$I_{m,k,j} = \frac{1}{\Delta x_k \Delta z_j} \int_{x_{k-1/2}}^{x_{k+1/2}} \mathrm{d}x \int_{z_{j-1/2}}^{z_{j+1/2}} \mathrm{d}z\, I_m(x,z) \quad (16)$$

$$I_{m,k\pm1/2,j} = \frac{1}{\Delta z_j} \int_{z_{j-1/2}}^{z_{j+1/2}} \mathrm{d}z\, I_m(x_{k\pm1/2},z) \quad (17)$$

$$I_{m,k,j\pm1/2} = \frac{1}{\Delta x_k} \int_{x_{k-1/2}}^{x_{k+1/2}} \mathrm{d}x\, I_m(x,z_{j\pm1/2}). \quad (18)$$

TCD
6, 4205–4231, 2012

Boundary conditions to Eq. (14) are as follows:

$$I_m(x_k, z_{J+1/2})|_{\cos\theta_m<0} = \frac{1}{4\pi} S_0, \tag{19}$$

$$I_m(x_k, z_{1/2})|_{\cos\theta_m>0} = \frac{A(x)}{\pi} \left\{ \sum_{\cos\theta_n<0} \Delta\Omega_n |\gamma_n| I_n(x_k, z_{1/2}) \right\}, \tag{20}$$

$$I_m(x_{1/2}, z_j)|_{\cos\phi_m>0} = A_s I_n(x_{1/2}, z_j)\big|_{\cos\phi_n = -\cos\phi_m}, \quad I_m(x_{K+1/2}, z_j)|_{\cos\phi_m<0} = 0. \tag{21}$$

To close the Eqs. (14)–(21) one needs additional relations. They are taken as

$$I_{m,k,j} = (1 - v_{m,k,j}) I_{m,k+s(\xi_m)/2,j} + v_{m,k,j} I_{m,k-s(\xi_m)/2,j}, \tag{22}$$

$$I_{m,k,j} = (1 - u_{m,k,j}) I_{m,k,j+s(\gamma_m)/2} + u_{m,k,j} I_{m,k,j-s(\gamma_m)/2}, \tag{23}$$

where the function $s(\xi) = \mathrm{sgn}(\xi) = \begin{cases} 1 & \text{as } \xi > 0, \\ -1 & \text{as } \xi < 0 \end{cases}$ and the weight parameters $v_{m,k,j}$, $u_{m,k,j}$ are of the segment [0,1]. They are chosen by estimation of gradient of solution being sought in a cell via preliminary computation in this cell with parameters

$$v_{m,k,j} = u_{m,k,j} = 1/2. \tag{24}$$

This means linear approximation to a solution in a cell, namely:

$$I_{m,k,j} = \left(I_{m,k+1/2,j} + I_{m,k-1/2,j}\right)/2 = \left(I_{m,k,j+1/2} + I_{m,k,j-1/2}\right)/2. \tag{25}$$

The resulting system of Eqs. (14)–(23) for the fixed node $\mathbf{\Omega}_m\{\theta_m, \phi_m\}$ consists of $3KJ + K + J$ equations for the same number of unknowns and can be solved by the iterative Seidel's method (Saad, 2000). This method is based upon decomposition of

TCD
6, 4205–4231, 2012

all quadrature nodes to four quadrants

$$W_1: \{(\theta_m,\phi_m),\ 0<\theta_m<\pi/2,\ 0<\phi_m<\pi\},$$
$$W_2: \{(\theta_m,\phi_m),\ 0<\theta_m<\pi/2,\ \pi<\phi_m<2\pi\},$$
$$W_3: \{(\theta_m,\phi_m),\ \pi/2<\theta_m<\pi,\ 0<\phi_m<\pi\},$$
$$W_4: \{(\theta_m,\phi_m),\ \pi/2<\theta_m<\pi,\ \pi<\phi_m<2\pi\}. \quad (26)$$

Eqs. (14)–(23) can be presented as

$$\hat{A}\, \boldsymbol{I}_m = \sum_{n=1}^{M} \rho_{nm}\, \boldsymbol{I}_n, \quad (27)$$

where the vector $\boldsymbol{I}_m$ contains all values of the mesh solution in the node $\boldsymbol{\Omega}_m\{\theta_m,\phi_m\}$. The explicit operator $\hat{A}$ corresponds to the differential operator in the left side of the Eq. (1). The coefficients ρ_{nm} are found using Eq. (9).

The Seidel's method is based upon the equations

$$\hat{A}\ (\boldsymbol{I}_m)^{it+1} - \rho_{mm}\ (\boldsymbol{I}_m)^{it+1} + \sum_{j=1}^{i-1} \sum_{n\in W_j} \rho_{nm}\ (\boldsymbol{I}_n)^{it+1} = \sum_{j=i}^{4} \sum_{n\in W_j, n\neq m} \rho_{nm}\ (\boldsymbol{I}_n)^{it}. \quad (28)$$

To inverse the operator $\hat{A}$ on $(it+1)$-th iterative step, the explicit upwind method is used, when values $I_{m,k+s(\xi_m)/2,j}$, $I_{m,k,j+s(\gamma_m)/2}$ and $I_{m,k,j}$ are found using known values $I_{m,k-s(\xi_m)/2,j}$, $I_{m,k,j-s(\gamma_m)/2}$ for a given node and a spatial cell.

Relative intensities of reflected radiation on the snow surface in the directions $\boldsymbol{\Omega}^*$ and $\boldsymbol{\Omega}^{**}$

$$\tilde{I}(z) = I(R,z,\boldsymbol{\Omega}^{**})/S_0, \quad \hat{I}(x) = I(x,H,\boldsymbol{\Omega}^{*})/S_0 \quad (29)$$

are of interest. Here the function $\hat{I}(x)$ defines the radiation intensity exiting from the top boundary of the system in the zenith direction $\boldsymbol{\Omega}^*$. The function $\tilde{I}(z)$ corresponds to

TCD
6, 4205–4231, 2012

radiation intensity reflected by the vertical side AB of the snowpack (see Fig. 5) in the direction $\mathbf{\Omega}^{**}$, perpendicular to the side AB.

Directions $\mathbf{\Omega}^{*}(\theta^{*},\phi^{*})$ and $\mathbf{\Omega}^{**}(\theta^{**},\phi^{**})$ are defined by visual angles θ^{*}, ϕ^{*} and θ^{**}, ϕ^{**}; they are not usually included into quadrature nodes in a general case. To find relative intensity in these directions with no interpolation, they are inserted into quadrature nodes with zero weights. It does not change solution values in other nodes.

The previous version of the presented algorithm was outlined by Sokoletsky et al. (2009), where it was applied for the calculation of solar light reflectance by natural sea waters. That time scattering phase functions were defined by their values in nodes of a very refined mesh over the interval [−1, 1] and approximated by piece-wise linear functions. Now scattering phase functions are given by their Legendre coefficients. Besides, the adaptive method of chosing additional meshes $\Omega_{j,m}$ to calculation of integrals (9) by Eq. (10) is applied, see Fig. 6.

4 Results

All computations were done by the code RADUGA-6 (Sokoletsky et al., 2009) on the hybrid cluster k100 (http://www.kiam.ru/MVS/resourses/k100.html) under the following parameters

1. the region height H m, the region semi-width $X = 1.85$ m, see Fig. 1;
2. the pit diameter D m, see Fig. 1;
3. the extinction coefficients $\sigma^{\text{snow}} = 1\ \text{mm}^{-1}$, $\sigma^{\text{air}} = 0.001\ \text{mm}^{-1}$;
4. the single scattering albedo $\omega_0^{\text{snow}}(z) \in [0.98, 1]$, $\omega_0^{\text{air}}(z) \equiv 1$;
5. the aerosol scattering phase function is obtained via the Mie's theory, the snow phase function is found by geometrical optics theory, see Fig. 7
6. both functions are decomposed into 800 Legendre polynomials;

TCD
6, 4205–4231, 2012

7. the diffuse source, when both a snowpack and a pit are covered by a sheer film;
8. number of nodes of the quadrature $M = 360$;
9. numbers of cells of the spatial meshes: $K = 468$, $J = 1610$. The mesh over z is refined in vicinity of the top boundary $z = H$, where intensity gradient is largest. The mesh over x is refined near snowpack side AB, see Fig. 5, for the same reason.

Both homogeneous and heterogeneous snowpacks are under consideration. A homogeneous snowpack is defined by the constant single scattering albedo ω_0^{snow}. A heterogeneous snowpack contains a polluted layer in a center of clear one, see Fig. 4:

$$\omega_0^{\text{snow}}(z) = \begin{cases} 0.98, \text{ as } \left|z - h/2\right| \le t/2, \\ \tilde{\omega}_0, \text{ as } \left|z - h/2\right| > t/2. \end{cases} \tag{30}$$

Here parameter t is thickness of a polluted layer, $\tilde{\omega}_0$ is albedo of the rest clearer snow.

The conditions of measurements define albedo of pit's bottom EB and albedo of left boundary EC (see Fig. 5).

1. no black film: $A_s = 1$, $A(x) = A^{\text{snow}} = 0.8$, see Fig. 1
2. a black film is only on the pit's bottom EB: $A_s = 1$, $A(x) = \begin{cases} 0 & \text{as } x \le R, \\ A^{\text{snow}} & \text{else.} \end{cases}$, see Fig. 2
3. a black film is on the pit's bottom EB and left boundary EC, see Fig. 3: $A_s = 0$, $A(x) = \begin{cases} 0 & \text{as } x \le R, \\ A^{\text{snow}} & \text{else.} \end{cases}$.

We consider relative radiation intensity on the vertical side AB of a snowpack, see Fig. 5, in the direction $\mathbf{\Omega}^{**}$, that is perpendicular to the side AB, and on the top boundary CD of the system in the zenith direction $\mathbf{\Omega}^{*}$.

TCD
6, 4205–4231, 2012

The relative intensity (see Eq. 29) at the horizontal line CD in the zenith direction $\mathbf{\Omega}^*$ for homogeneous snowpacks is given in Fig. 8. One can see that the intensity of reflected radiation has extrema near the air/snow boundary; similar effects are observed in clouds illuminated by direct solar light (Nikolaeva et al., 2005). In the problem under study maximum of radiation intensity in snow near air/snow boundary is formed by radiation penetrating in the snowpack and poorly absorbed near the boundary; maximum enhances as snow absorption enhances. In a similar way minimum of radiation intensity arises in air near the air/snow boundary due to absorption of radiation by snow.

The relative intensity $\tilde{I}(z)$ at the vertical side AB of a snowpack is used to retrieve optical parameters of snow. Retrieval algorithms are based upon 1-D models of radiation transport, that assume the radiation intensity reflected by vertical side AB of a homogeneous snowpack is a constant function of depth z, at least far from the top and bottom boundary of a snowpack (i.e. points A and B, see Fig. 5).

The calculated relative radiation intensity $\tilde{I}(z)$ of the homogeneous snowpack is presented in Fig. 9–13 for various values of single scattering albedo ω_0^{snow}, hole depth H, hole diameter $D = 2R$ and surface albedos $A(x)$ and A_s. Besides these figures give the function $r(z)$, defining the deviation of the function $\tilde{I}(z)$ from its value in the center point in percent

$$r(z) = 100 \left[1 - \tilde{I}(z)/\tilde{I}(h/2)\right] \ \%. \tag{31}$$

It follows from Fig. 9 that the deviation $r(z)$ is less varying if the smaller part of the pit is covered by a black film. Variation $r(z)$ decreases due to reflection of radiation by bottom and opposite side of the pit.

Figure 10–13 correspond to the pit with no black film. Here variation of the deviation $r(z)$ is smaller. It does not tend to zero as sizes (depth and diameter) of the pit increase. Decrease of variation of the deviation $r(z)$ with increase of the diameter D stops under definite value of D, see Fig. 11. The function $r(z)$ depends weakly on the pit's depth H (see Fig. 12), and essentially increases as absorption in snow amplifies (see Fig. 10).

TCD
6, 4205–4231, 2012

Clearly, the 1-D models can not be applied to find the relative intensity $\tilde{I}(z)$ under any sizes of a pit.

Influence of heterogeneity of a snowpack on relative radiation intensity is showed in Fig. 10 and Fig. 13. The thin polluted layer in center of pure snowpack, see Fig. 4, leads to minimum in reflected radiation intensity in the vicinity of the layer. Note although the strong minimum is concentrated near the polluted layer, shadow of the minimum is spread over the whole side, if absorption is weak enough. This fact impedes the use of the 1-D models to simulate the relative intensity $\tilde{I}(z)$.

5 Conclusions

We consider 2-D problems on reflecting solar light by rectangular wide pit in a thick snow layer. Simulation (by the parallel code RADUGA-6) is based upon the mesh technique of the discrete ordinate method under exact treating complicated peaked scattering phase functions of solar radiation by snow crystals and aerosol particles. The diffuse radiation source, produced by a film covering a snowpack, is under consideration. Such source models are close to those for real ground measurements.

2-D effects in reflected in zenith radiation intensity (brightening and shadowing) near vertical side of the pit are significant in spite of diffuse radiation source.

2-D effects are significant on the vertical side of the pit. First the relative intensity of radiation on the vertical wall is formed via reflection by both sides of a pit and its bottom. Then intensity radiation reflected by a homogeneous snowpack is not constant function of the depth even for a very wide pit. Besides, the slope of this function increases as absorption of light in snow enhances.

Additional 2-D effects arise in layered snowpacks. Although minimum in intensity on a vertical side of a pit is localized near a polluted layer, intensity out of minimum can be influenced by this polluted layer.

One can conclude 1-D models can lead to larger errors in the simulation of the measured radiation intensity on vertical walls of snowpits.

TCD
6, 4205–4231, 2012

Acknowledgements. The work is supported by research program N 14 of Presidium of Russian Academy of Sciences. A. Kokhanovsky thanks BMBF Project CLIMSLIP for the support of this work and also to M. Schneebeli for the suggestion to conduct this study. O. Nikolaeva thanks L. P. Bass for the useful discussions.

References

Arnaud, L., Picard, G., Champollion, N., Domine, F., Gallet, J. C., Lefebvre, E., Fily, M., and Barnola, J. M.: Measurement of vertical profiles of snow specific surface area with a 1cm resolution using infrared reflectance: instrument description and validation, J. Glaciol., 57, 201, 17–29, 2011.

Barker, H. W. and Korolev, A. V.: An update on blue snow holes, J. Geophys. Res., 115, D18211, doi:10.1029/2009JD013085, 2010.

Kokhanovsky, A. A., Rozanov, V. V., Aoki, T., Odermatt, D., Brockmann, C., Krúger, O., Bouvet, M., Drusch, M., and Hori, M.: Sizing snow grains using backscattered solar light, Int. J. Remote Sens., 32, 6975–7008, 2011.

Matzl, M. and Schneebeli, M.: Measuring specific surface area of snow by near-infrared photography, J. Glaciol., 52, 558–564, 2006.

Nikolaeva, O. V., Bass, L. P., Germogenova, T. A., Kokhanovsky, A. A., Kuznetsov, V. S., and Mayer, B.: The influence of neighbouring clouds on the clear sky reflectance studied with the 3-D transport code RADUGA, J. Quant. Spectrosc. Ra., 94, 405–424, 2005.

Painter, T. H., Molotch, N. P., Cassidy, M., Flanner, M., and Steffen, K.: Contact spectroscopy for determination of stratigraphy of snow optical grain size, J. Glaciol., 53, 121–127, 2007.

Saad Y.: Iterative Methods for Sparse Linear Systems, University of Minnesota, Minneapolis, 2000.

Sokoletsky, L. G., Budak, V. P., Bass, L. P., Nikolaeva, O. V., Lunetta, R. S., Kuznetsov, V. S., and Kokhanovsky, A. A.: A comparison of numerical and analytical radiative transfer solutions for plane albedo in natural waters, J. Quant. Spectrosc. Ra., 110, 1057–1206, 2009.

TCD

6, 4205–4231, 2012

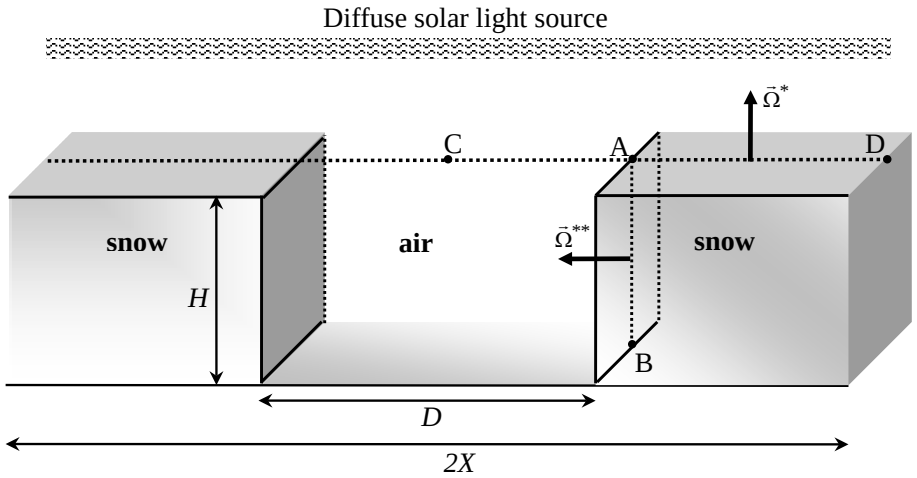

Fig. 1. The real 3-D geometry of the region with no black film.

TCD
6, 4205–4231, 2012

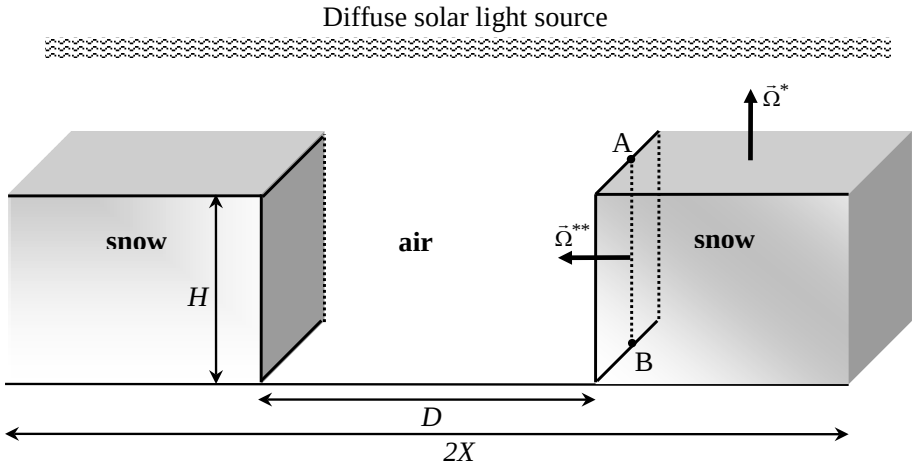

Fig. 2. The real 3-D geometry of the region with black film on the pit's bottom.

TCD
6, 4205–4231, 2012

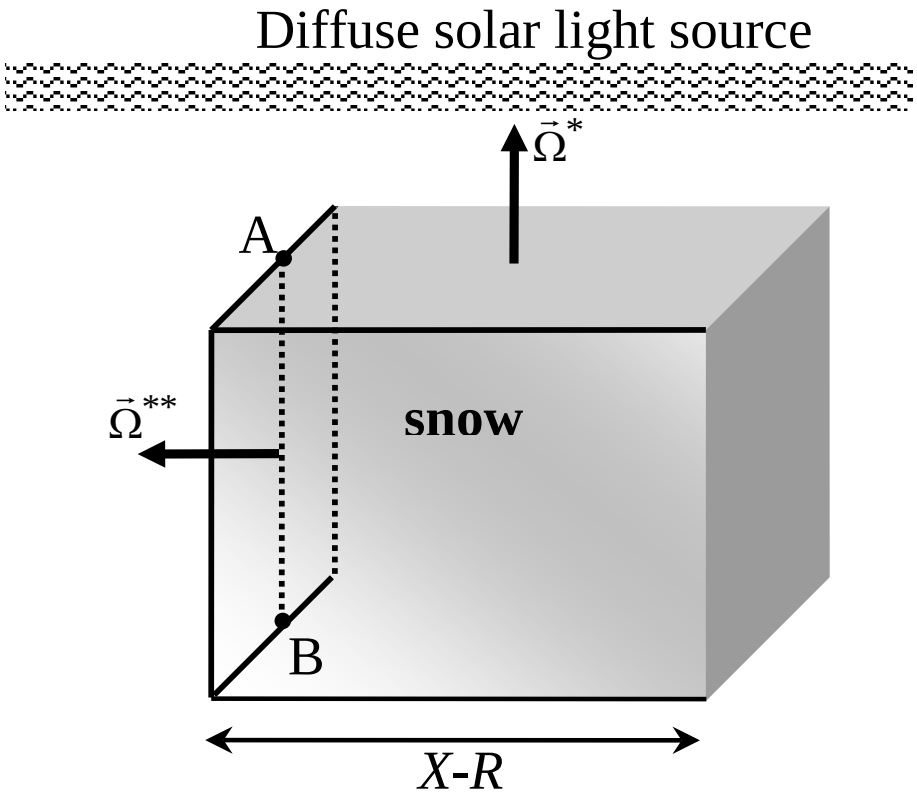

Fig. 3. The real 3-D geometry of the region with black film on the bottom and the opposite side of the pit.

TCD
6, 4205–4231, 2012

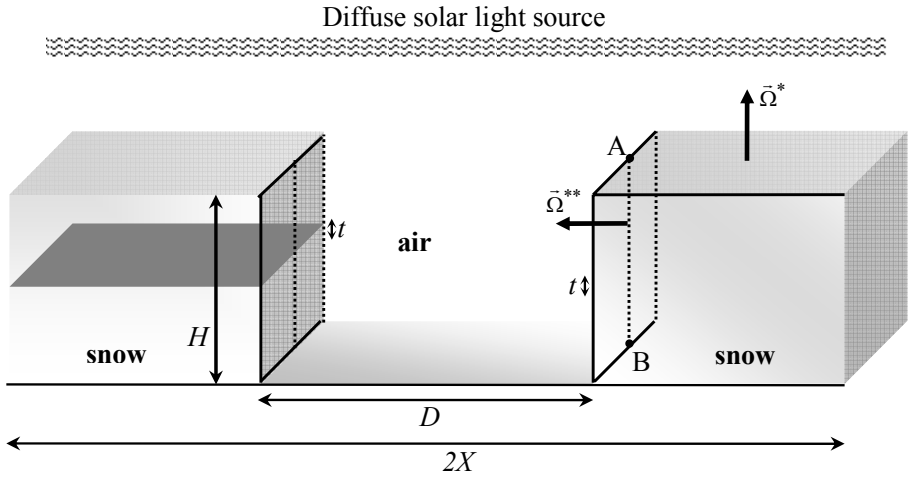

Fig. 4. The real 3-D geometry of the region with the central polluted layer.

TCD
6, 4205–4231, 2012

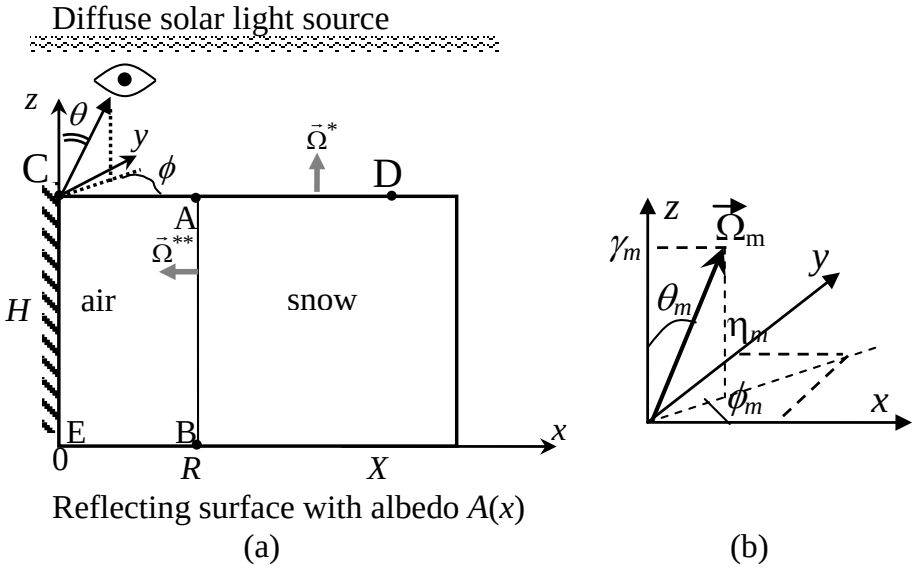

Fig. 5. The 2-D region with wide rectangular pit and observation direction angles θ and ϕ.

TCD
6, 4205–4231, 2012

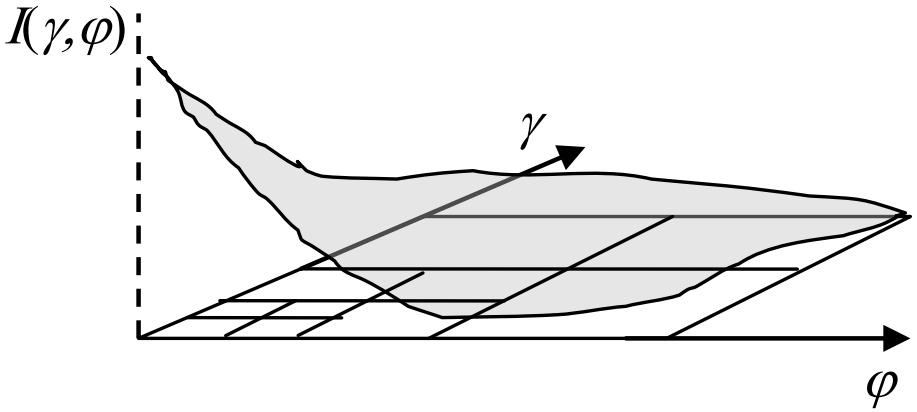

Fig. 6. Example of an additional quadrature on a angular nodes adapted to a function being integrated.

TCD
6, 4205–4231, 2012

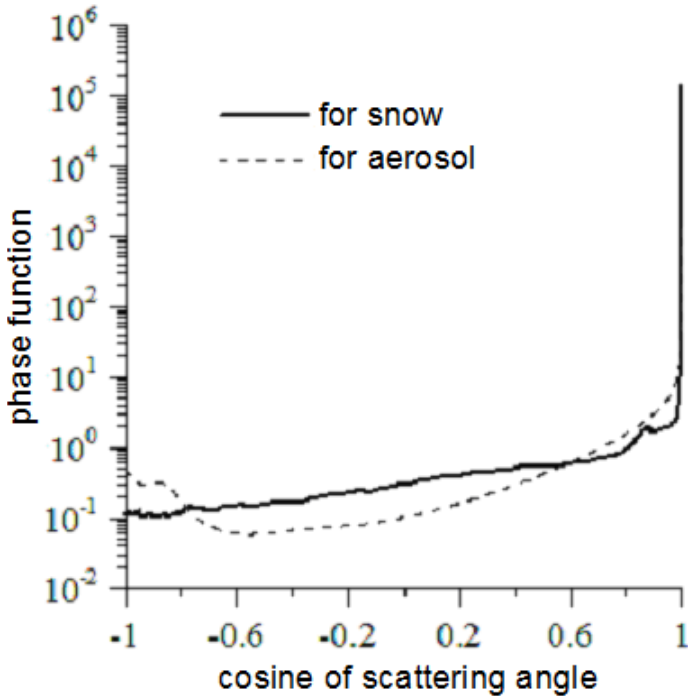

Fig. 7. The scattering phase functions.

TCD
6, 4205–4231, 2012

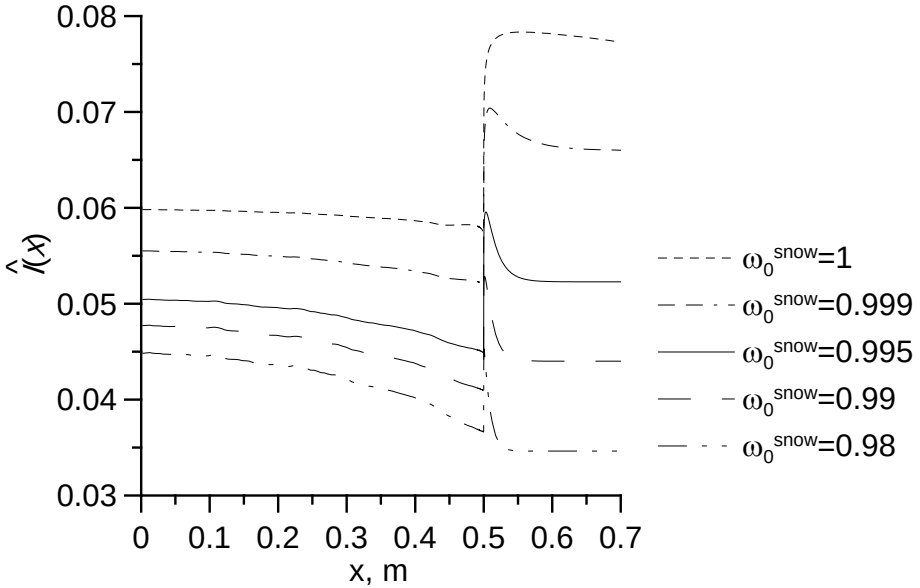

Fig. 8. Relative intensity $\hat{I}(x)$ in the zenith direction $\mathbf{\Omega}^*$ on the top boundary CD of the snowpack for the various single scattering albedos $\omega_0^{snow}(z)$. It was assumed that the diameter D = 1 m, depth H = 0.7 m and snow surface albedo A^{snow} = 0.8.

TCD
6, 4205–4231, 2012

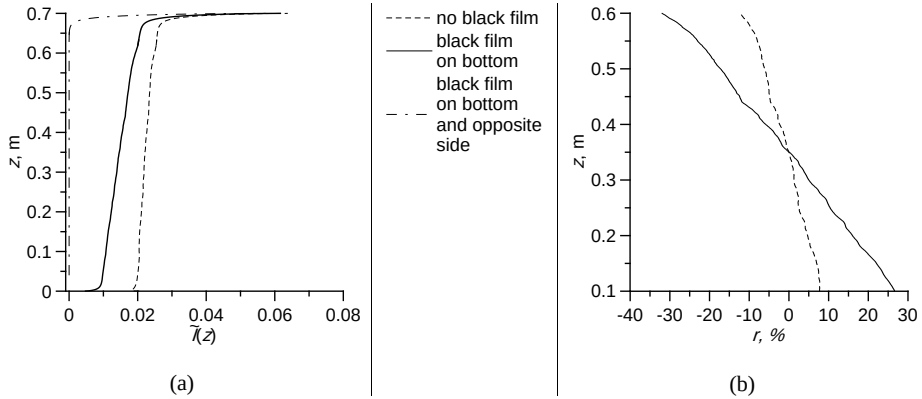

Fig. 9. Relative intensity $\tilde{I}(z)$ in the direction $\mathbf{\Omega}^{**}$ **(a)** and the deviation $r(z)$ (in percent, see Eq. 31) **(b)** on the vertical side AB of the snowpack at the snow single scattering albedo $\omega_0^{\text{snow}} = 0.98$, the diameter $D = 1\,\text{m}$ and depth $H = 0.7\,\text{m}$ for various albedos at the bottom and opposite side of the pit.

TCD
6, 4205–4231, 2012

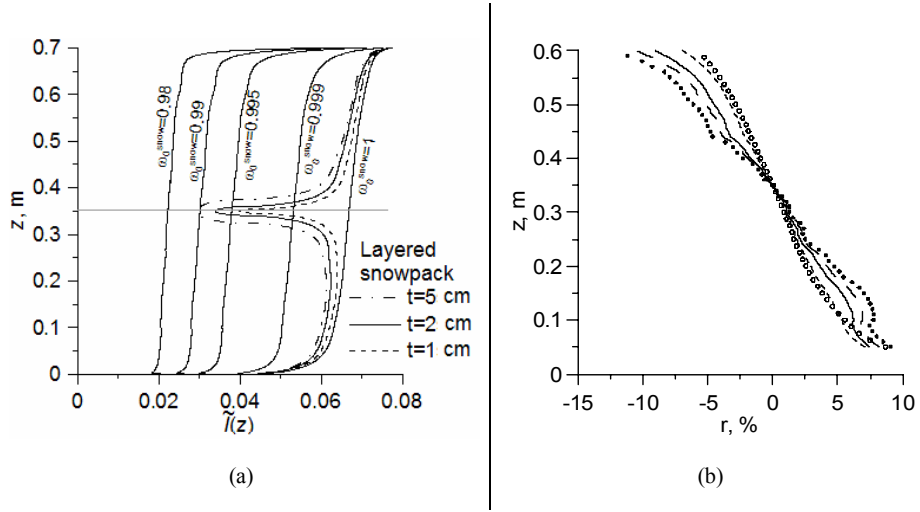

Fig. 10. Relative intensity $\tilde{I}(z)$ in the direction $\mathbf{\Omega}^{**}$ **(a)** and the deviation $r(z)$ (in percent, see Eq. 31) **(b)** on the vertical side AB of the snowpack for homogeneous and layered snowpacks with $\tilde{\omega}_0 = 1$. Diameter $D = 1$ m, depth $H = 0.7$ m and snow surface albedo $A^{\text{snow}} = 0.8$.

TCD
6, 4205–4231, 2012

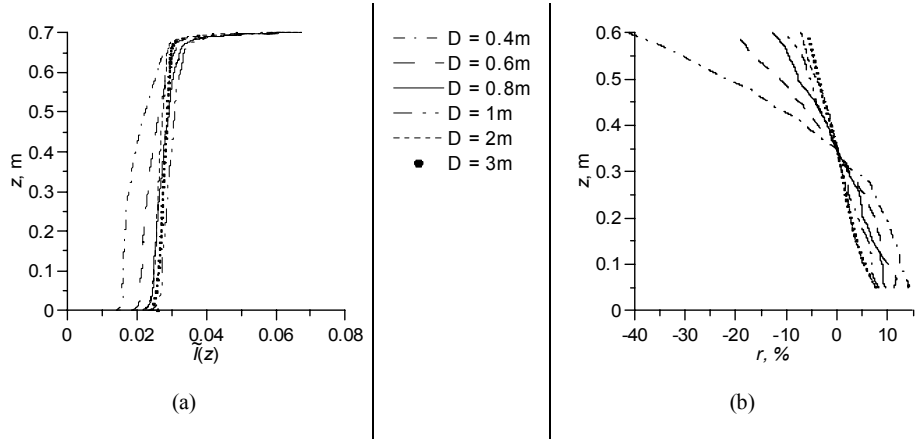

Fig. 11. Relative intensity $\tilde{I}(z)$ in the direction $\mathbf{\Omega}^{**}$ **(a)** and the deviation $r(z)$ (in percent, see Eq. 31) **(b)** on the vertical side AB of the snowpack at the snow single scattering albedo $\omega_0^{\text{snow}} = 0.98$, the depth $H = 0.7$ m and snow surface albedo $A^{\text{snow}} = 0.8$ for different diameters D.

TCD
6, 4205–4231, 2012

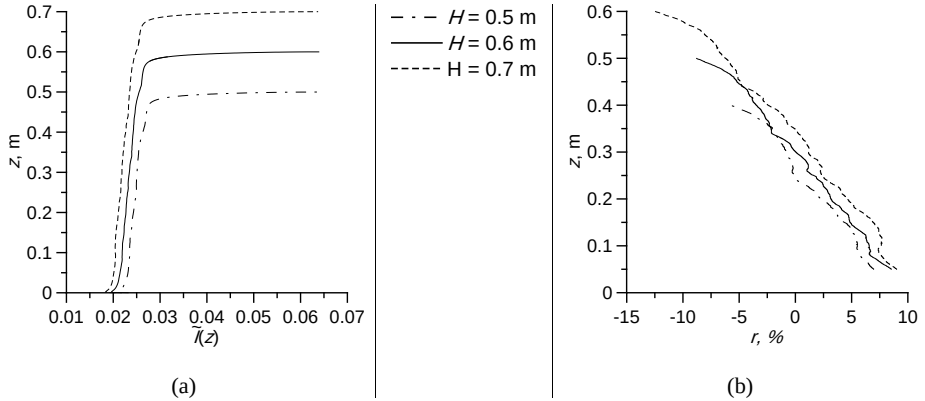

Fig. 12. Relative intensity $\tilde{I}(z)$ in the direction $\mathbf{\Omega}^{**}$ **(a)** and the deviation $r(z)$ (in percent, see Eq. 31) **(b)** on the vertical side AB of the snowpack at the snow single scattering albedo, $\omega_0^{\text{snow}} = 0.98$, the diameter $D = 1$ m and snow surface albedo $A^{\text{snow}} = 0.8$ for various values of the depth H.

TCD
6, 4205–4231, 2012

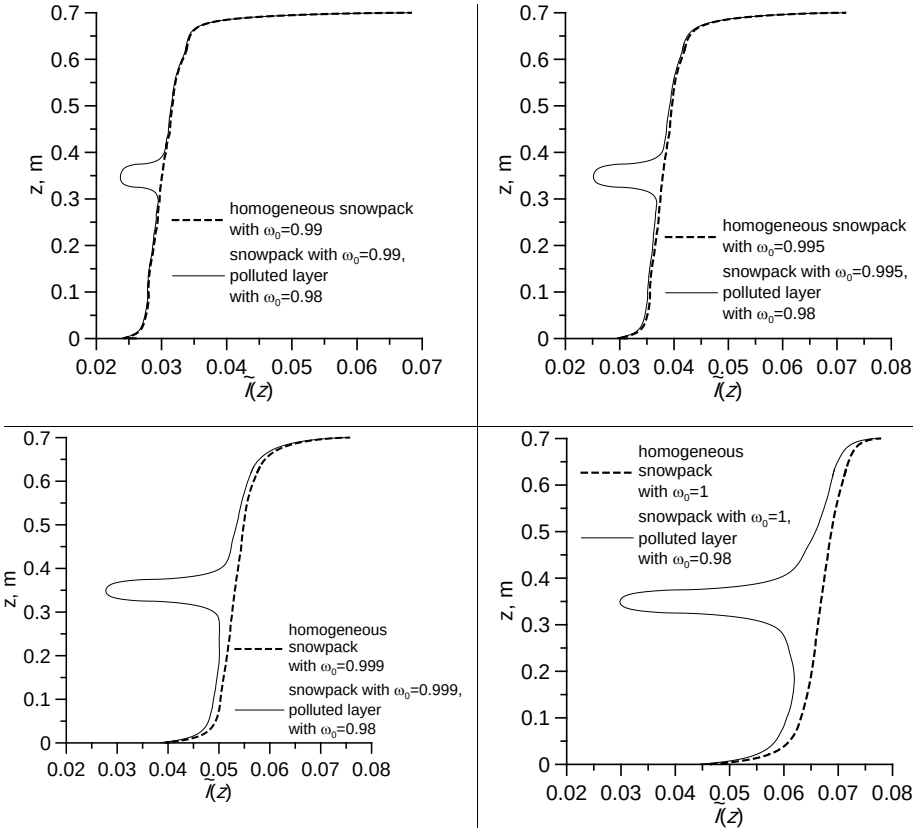

Fig. 13. Relative intensity $\tilde{I}(z)$ in the direction $\mathbf{\Omega}^{**}$ on the vertical side AB under diameter D = 1 m, depth H = 0.7 m and snow surface albedo A^{snow} = 0.8 for different layered snowpacks, when thickness of the polluted layer is 5 cm.

TCD
6, 4205–4231, 2012